Molecular Physics
Vol. 108, Nos. 21–23, 10 November–10 December 2010, 3147–3166

Taylor & Francis
Taylor & Francis Group

INVITED ARTICLE

Electronic structure of solids with WIEN2k

Karlheinz Schwarz[a]*, Peter Blaha[a] and S.B. Trickey[b]

[a]*Institute of Materials Chemistry, Vienna University of Technology, Vienna, Austria;*
[b]*Quantum Theory Project, University of Florida, Gainesville, Fl, USA*

(*Received 5 May 2010; final version received 24 June 2010*)

Aspects of the progress over the last 40–50 years in calculating the electronic structure of solids and surfaces are sketched in the context of collaboration on the code now called WIEN2k. Different facets that are relevant for material sciences are discussed, ranging from quantum mechanics to the augmented plane wave (APW) method, as well as improvements in computer hardware and algorithms and related numerical accuracy. In this long period, the complexity and realism of applications to condensed matter systems has significantly increased and many properties which are closely related to experiments can now be calculated. This progress is illustrated by the fact that WIEN2k now is used worldwide by more than 1600 groups. The major steps in this development are illustrated for a few selected examples.

Keywords: quantum mechanics; density functional theory; augmented plane wave method; WIEN2k; solids; surfaces

1. Introduction

In the study of advanced materials, several characteristics, e.g. structure, composition, disorder, temperature or pressure determine the properties of interest. Solid materials are of great technological importance of course, but the challenge to theory and computation is that they are governed by very different length and time scales. These may differ by many orders of magnitude depending on the specific applications. On the length scale from meters (m) down to micrometers (μm) classical mechanics and continuum models are the dominant conceptual framework for investigation of diverse material properties. However, when one comes to the nanometer (nm) scale or atomic dimensions measured in Å, all properties are determined (or critically influenced) by the electronic structure of the solid. In the development of modern materials, understanding on the atomic scale frequently is essential in order to replace trial and error procedures by a systematic design. Modern devices in the electronic industry provide an example. In them, the relentless pursuit of miniaturization is one of the key advances. Other applications are found in the area of magnetic recording or other storage media (see for example the Nobel prizes in physics for Fert and Grünberg in 2007 [1]). All these advances are intimately connected to quantum mechanical aspects of the materials.

One possible way to study complex systems (which may contain many atoms) is to perform computer simulations. In general, calculations of solids (metals, insulators, minerals, etc.) or surfaces can be performed with a variety of methods ranging in refinement from classical to quantum mechanical (QM) approaches. Classical atomistic treatments usually rely upon force fields. In these, the forces of interaction between the atoms are parameterized in such a way as to reproduce a selected set of pertinent experimental data such as equilibrium geometries, bulk moduli or vibrational frequencies (phonons). These schemes have reached a high level of sophistication and are often useful within a given class of materials provided good parameters are already known from closely related systems. Implicitly a parameterized force field is an empirical approximation for a single Born–Oppenheimer potential energy surface. As such, it cannot represent chemical bond formation or breaking, both of which are crucial to the modification of material properties. Moreover, if force field parameters are not available, or if a system shows unusual phenomena that are not yet understood, one often must rely on so-called first-principles (or *ab initio*) calculations. (These two terms have subtly different meanings in condensed matter and materials physics compared to quantum chemistry. We use it in the former sense to mean a well-defined model with no adjustable parameters.) Such calculations have more demanding computer requirements

*Corresponding author. Email: kschwarz@theochem.tuwien.ac.at

ISSN 0026–8976 print/ISSN 1362–3028 online

DOI: 10.1080/00268976.2010.506451
http://www.informaworld.com

than classical or semi-empirical simulations and thus only can treat comparatively smaller units. The advantage of first-principles methods lies in the fact that they do not require any experimental knowledge (beyond chemical composition) to be carried out. The following presentation will be restricted to first-principles methods whose main characteristics shall be outlined briefly.

Here we focus on the atomic scale. For it, one often starts with an ideal crystal that is studied at zero temperature. The unit cell contains several atoms (with their nuclei at specified positions) and is repeated with periodic boundary conditions. Quantum mechanics governs the electronic structure that is responsible for properties such as relative stability, chemical bonding, relaxation of the atoms, phase transitions, electrical, mechanical, optical or magnetic behaviour, etc. Corresponding first principles calculations are mainly done within Density Functional Theory (DFT), according to which the many-body problem of interacting electrons and nuclei is mapped to a series of one-electron equations, the so-called Kohn–Sham (KS) equations. For the solution of the KS equations several methods have been developed, with the Linearized-Augmented-Plane-Wave (LAPW) method being among the most accurate. During the last 30 years we have developed a computer code – WIEN2k – that is now used worldwide to solve crystal properties on the atomic scale (see www.wien2k.at).

Our presentation is oriented around that formulation and code. The paper is organized as follows: Section 2 describes the quantum mechanical aspect (from the Xα method to DFT), Section 3 summarizes the major steps in the development of the augmented plane wave (APW) method and its improvements; Section 4 sketches key parts of the dramatic improvement of computers during the last 50 years; Section 5 highlights the equally important algorithmic developments and related issues of numerical accuracy; Section 6 discusses various properties that are derived from the electronic structure of a condensed matter system and illustrates them via selected examples of published research; Section 7 outlines the strategy behind the code distribution, and Section 8 summarizes the progress that has been made and gives a short conclusion. Occasional relevant personal observations are interspersed.

2. Quantum mechanics

Because electrons are indistinguishable Fermions, their wave functions must be antisymmetric when two electrons are interchanged. This requirement leads to the phenomenon of exchange (in addition to correlation, which occurs because of the Coulomb interaction). The traditional approach was to begin with the Hartree–Fock (HF) approximation. It is a variational wave-function description (with one Slater determinant). The HF equations have the computational disadvantage that each electron moves in a different potential. Exchange is treated exactly but correlation effects are omitted by definition. The latter can be included by more sophisticated approaches such as configuration interaction (CI) or coupled cluster (CC) schemes [2]. But such refinements progressively require more computer time as the system size (N, proportional to the number of electrons) grows, with a scaling as bad as N^7. As a consequence, only relatively small systems (on the scale of condensed matter) can be treated but – where applicable – high accuracy can be reached.

2.1. *The statistical exchange (Xα and X$\alpha\beta$ method)*

A bit of history is helpful. In this context the reader is referred to the review by J.W.D Connolly [3]. To simplify the HF equations, which 50 years ago were too difficult to solve for solids, one can approximate the HF-exchange energy density locally by the exchange energy

$$E_{\mathrm{XS}} = -(3/8\pi)^{1/3} \int \rho(r)^{4/3} \mathrm{d}r \qquad (1)$$

of the homogeneous electron gas. Thus, in 1951 Slater [4] proposed replacement of the non-local HF exchange by the statistical exchange, called Slater's exchange. Here ρ is the electron number density (in casual use, the density). The variational one-electron equations then lead

$$V_{\mathrm{XS}}(r) = -6[(3/8\pi)\rho(r)]^{1/3} \qquad (2)$$

to a local exchange potential.

Subsequently Gaspar [5] and Kohn and Sham [6] proposed an alternative approximate exchange potential which differs from V_{XS} only by a factor of 2/3. Solid state calculations based on these two approximations often bracketed the corresponding experimental results. As a matter of computational exploration in the late 1960s, it was easy to modify existing band-structure programs to allow for a coefficient from 2/3 to 1 multiplying the right hand side of Equation (1). Systemization of this exploration led to the development of the Xα method [7], in which the range of α is between 2/3 and 1. In the early 1970s the corresponding α parameters were optimized for the atoms [8,9]. These parameters were widely used, mainly in the

solid state community, with many successes (and some notable failures; see below). The reason for the success of the Xα method was its combination of simplicity and surprising accuracy, which in many cases exceeds that of the HF scheme that Xα supposedly approximated. From the perspective of modern DFT, one among several reasons for this success is that the spherically averaged exchange-correlation (XC) hole is the essential ingredient in the DFT XC energy. Despite the oversimplification of the Xα ansatz, the spherically averaged Xα exchange hole actually resembles the true exchange-correlation hole and better than HF. In fact, nowadays Xα is most systematically understood as a simple, one-parameter approximate XC functional which scales as exchange-only (see next section).

In compounds which contain several atoms, different α parameters had to be used. An early attempt was made to construct a Z-independent statistical exchange potential by including a gradient term, called the X$\alpha\beta$ method [10]. Although this scheme was more general than the Xα scheme, X$\alpha\beta$ was not commonly accepted at that time, in contrast to the generalized gradient approximations (GGA) discussed later.

The interpretation of the orbital energies ε_i differs between HF and Xα, since in HF they can be interpreted as approximate ionization energies in consequence of Koopmans' theorem [11]. In contrast, the Xα eigenvalues correspond to the partial derivatives of the total energy with respect to occupation numbers (the Slater–Janak theorem [12]). This property can be utilized for example in Slater's transition state concept [13] to estimate core energies. In it, one calculates the core eigenvalues with half a core electron removed and then the partial derivative much better resembles the slope $\Delta E/\Delta N$ as in Koopmans' theorem for HF. The reader is also referred to a more recent discussion on the Slater–Janak theorem [14].

2.2. *Density functional theory (DFT) and the Kohn–Sham equations*

By now, the predominant scheme for calculating the electronic properties of solids is based on DFT, for which Walter Kohn (born in Vienna) received the Nobel Prize in chemistry in 1998. DFT is a universal approach to the quantum mechanical many-body problem. In 1964 Hohenberg and Kohn [15] showed that the total energy E of an interacting inhomogeneous electron gas in the presence of an external potential (given by the nuclei) is a functional of the electron density ρ. Moreover, ρ uniquely parameterizes the variational principle for the total energy E of the system. In the conventional way of implementing the variation principle in DFT, the system of interacting electrons is mapped uniquely onto an effective non-interacting system with the same total density. Specifically, Kohn and Sham [6] decomposed the unknown variational functional further:

$$E = T_s[\rho] + \int V_{\text{ext}}\rho(\vec{r})\mathrm{d}\vec{r} + \frac{1}{2}\int \frac{\rho(\vec{r})\rho(\vec{r}')}{|\vec{r}' - \vec{r}|}\mathrm{d}\vec{r}\,\mathrm{d}\vec{r}' + E_{\text{xc}}[\rho]. \tag{3}$$

The four terms (for an atom) correspond to the kinetic energy of the non-interacting electrons, the nuclear-electronic interaction energy E_{ne}, the Coulomb energy (including the self-interaction) and the exchange-correlation energy E_{xc}. At this point, Equation (3) is still exact. From a numerical point of view one should note that the first three terms are large numbers while the last is essential but small and thus can be approximated. The main idea of Kohn–Sham [6] was to introduce orbitals to calculate the non-interacting kinetic energy (the first term) accurately. This is a major improvement over the Thomas Fermi model. By applying the variational principle one obtains the Kohn–Sham (KS) equation

$$\left[-\frac{1}{2}\nabla^2 + V_{\text{ext}}(\vec{r}) + V_C\big[\rho(\vec{r})\big] + V_{\text{xc}}\big[\rho(\vec{r})\big]\right]\Phi_i(\vec{r}) = \varepsilon_i\,\Phi_i(\vec{r}), \tag{4}$$

according to which the non-interacting particles of the auxiliary system move in an effective local one-particle potential. The four terms in Equation (4) (written for an atom with the obvious generalization to molecules and solids) are, in order, the kinetic energy operator, the external potential from the nucleus, the electron-electron Coulomb potential, and the exchange-correlation potential V_{xc}. The first three terms comprise a classical mean-field (Hartree) description (except for the implicit Fermion character of the density). Quantum mechanics arises explicitly in the XC potential, V_{xc}, which is the functional derivative of the XC energy with respect to the density. In principle it incorporates exchange and all correlation effects exactly. The KS equation [6], must be solved iteratively until self-consistency is reached. In the KS scheme the electron density is obtained by summing over all occupied states, i.e. by filling the KS orbitals (with increasing energy) according to the aufbau principle,

$$\rho(\vec{r}) = \sum_i^{\text{occ}}\big[\phi_i(\vec{r})\big]^2. \tag{5}$$

(In solids there are occupation numbers to account for state labelling, namely the k-points in the Brillouin Zone and the band index n.)

The exact functional form of the exchange-correlation energy, and hence the potential V_{xc}, is not known, so one needs to make approximations. After the Kohn–Sham–Gaspar approximation [5,6] already mentioned, early applications were done by using results from quantum Monte Carlo calculations for the homogeneous electron gas, for which the problem of exchange and correlation can be solved exactly, leading to the modern local density approximation (LDA) [16]. LDA works reasonably well but has some shortcomings mostly due to its tendency to overbind, which often causes shortened lattice constants relative to experiment. Modern XC approximations, especially those using the generalized gradient approximation [17] (GGA), often improve upon LDA by introducing dependence on the gradient of the electron density. A famous example was iron, for which LDA gives a lower energy for non-magnetic fcc Fe than for ferromagnetic bcc Fe, whereas GGA correctly predicts that the magnetic bcc Fe (at nearly the experimental volume) is more stable than fcc Fe. The main advantage is that these schemes allow calculating the electronic structure of complex systems containing many atoms such as very large molecules or solids.

There is extensive literature about DFT, which we do not attempt to cover here. After LDA and GGA, meta-GGA functionals were proposed (for example in [18]), which depend not only on the density and its gradient, but also on the kinetic energy density τ.

For a long time the Perdew–Burke–Ernzerhof (PBE) [17] version was believed to be the 'best' GGA, but now new types of GGAs have been developed which perform better, at least for certain properties. For instance it is well known that the PBE-GGA overestimates lattice constants of solids (except for 3d systems), while new functionals tailored towards solids can significantly reduce the typical errors below half a percent [19,20]. It should be mentioned, however, that for other properties (like atomization energies of small molecules) such special functionals cause larger deviations from experimental values.

There are well-documented cases for which DFT calculations with an approximate XC functional disagree even qualitatively with experimental data and lead, for instance, to prediction of a metal instead of an insulator. For these so-called highly correlated systems, one typically must go beyond comparatively simple DFT approximations. This is an area of active research. One of these choices to treat local correlation beyond a simple XC functional is the use of a Hubbard U [21] for localized one-electron states in combination with LDA or GGA for the rest. This approach is generically called LDA + U. In it, one explicitly includes the on-site Coulomb repulsion between the localized orbitals (often f-electrons or late transition metal d-orbitals). Applications will be discussed in connection with the double perovskite $YBaFe_2O_5$ (Section 6.3) or PrO_2 (Section 6.6).

Another approach is the use of a hybrid functional. In those, a fraction of single-determinant exchange (in casual usage, HF exchange) is mixed with a GGA [22]. While the complete calculation of single-determinant exchange is rather expensive for solids, for localized orbitals a much cheaper but still reasonably accurate solution exists, namely to treat on-site exact exchange only for these orbitals [23].

Although the KS one-electron eigenvalues have no general formal standing as excitation energies, they are often used that way in order to estimate spectroscopic (optical) properties. The observation that the energy gap for insulators or semiconductors from simple DFT approximations typically is underestimated by 50% was already known from early APW calculations with Xα [24]. This topic is discussed in more detail in Section 6.7.

It should be stressed that modern DFT-codes can solve the KS equations very accurately and the quality of the results depends solely on the choice of the XC functional used in the calculations. In order to solve the KS equations many computer programs are available. Most of them use a variational method with some kind of basis set. In LCAO (linear combination of atomic orbitals) type schemes, Gaussian or Slater type orbitals (GTOs or STOs) are used. GTO-basis methods are predominant in molecular calculations but comparatively rare in periodic system codes. *Personal aside:* In a bit of irony, after working on the original WIEN code, S.B.T. was compelled by administrative duties to reduce his research scope and he continued work only on GTO-basis methods for solids and surfaces. [25]. But in solids, plane wave (PW) basis sets with or without augmentation provide a more natural basis set which sometimes is characterized as being unbiased because it can be enlarged simply going to higher plane waves. Other methods beside LAPW make use of muffin-tin orbitals (MTOs), for example, LMTO (linear combination of MTOs) [26] or ASW (Augmented Spherical Wave) [27]. In the former cases, the basis functions are given in analytic form, but in the latter the radial wave-functions are

obtained numerically by integrating the radial Schrödinger equation.

The pseudopotential approximation is closely related to the use of plane-wave-type basis sets. In it, the all-electron orbitals are replaced by node-less pseudo-orbitals. For the latter, plane waves are very well-suited and efficient bases to which efficient fast Fourier techniques can be applied (see for example the book by D.J. Singh [28]). Various schemes all have advantages and disadvantages but in the following we will just focus on the all-electron augmented plane wave (APW) based method that is the basis of the WIEN2k code.

Personal aside: In January 1969, S.B.T. joined the Quantum Theory Project as a part of Professor Slater's group. With a background in 'quantum crystals' (solid He and H lattice dynamics), he had to learn Xα and 'band-structure' methods. As a graduate student he had struggled with Kohn's DFT paper in the 1965 Tokyo Summer School Lectures book [29]. So it slowly became clear to him that Xα is a form of approximate DFT, not a universally shared view at the time. In summer 1969, K.S. (the first author, *not* Kohn-Sham!), who had used the APW method for his recently finished thesis, came to Gainesville to work with Professor Slater. The two of us soon became friends and collaborators. Thus began the saga which this article recounts. Our work was with the APW method, which we summarize next.

3. The augmented plane wave (APW) based methods

Among the most accurate schemes for solving the KS equations is the all-electron full-potential linearized-augmented-plane-wave (FP-LAPW) method on which the WIEN code is based. The original version was published in 1990 [30]. It was the first LAPW code to be made generally available for other users. In this section we sketch the major steps in the program development which led to the present WIEN2k code (now used worldwide by more than 1600 groups). The perspective is personal and not that of a complete survey of all the literature in this context.

3.1. *The original APW method*

As far back as 1937 Slater proposed the APW method [31]. In it the unit cell is partitioned into (non-overlapping) atomic spheres that are centred at the atomic sites (region I) and an interstitial region (II), for which different basis functions are used. For the construction of these functions the *muffin tin* approximation (MTA) is used, i.e. the potential is assumed to be spherically symmetric within each atomic sphere but constant outside. Atomic-like functions are used in region I but plane waves in region II. Each plane wave is augmented by corresponding atomic partial waves, i.e. atomic-like solutions inside each atomic sphere consisting of a radial function u_ℓ times spherical harmonics.

It is useful to recall the crude way such calculations had to be done at that time (before 1968) in order to see the enormous progress that has been made since. Details are in the marvelous but nearly forgotten review by Mattheiss, Wood, and Switendick [32].

To summarize how it was in the late sixties, the potential was of muffin tin form and was constructed as superposition of free atomic potentials (Mattheiss' construction [32]). No SCF procedure was performed and thus the results depended on various details such as choice of sphere radii, atomic configuration (e.g. Cu $3d^9 4s^2$ or $3d^{10} 4s^1$) or assumed ionicity. Nevertheless the calculations were demanding, because one had to solve a non-linear eigenvalue problem, since the radial basis functions in APW depend on the one-electron energy. One first had to choose a set of trial energies for those eigenvalues, then solve the radial Schrödinger equation for those energies to obtain the basis functions. Then one had to construct the Hamiltonian and overlap (H and S) matrixes, whose corresponding secular determinant |H-ES| should vanish but in general did not (because the trial eigenvalues were not correct). The energy eigenvalues had to be found numerically by changing the trial energy and finding the zeros of the determinant. (The procedure is summarized in [33].) However, an important advantage of APW is that it leads to the exact solution for the MTA. In this context, note the lengthy discussions in Mattheiss, Wood, and Switendick [32] on finding the eigenvalues (and the appendix on logarithmic derivatives), on symmetrization, and on corrections to the MTA. Especially noteworthy is the fact that they leave self-consistency to the last section. *Personal aside:* As mentioned, K.S. had used the APW method already in his PhD thesis and applied it to the two compounds ScC and ScN, which crystallize in the sodium chloride structure [34]. In contrast, S.B.T. had to learn the method and code. His teachers were K.S., Jim Conklin, Frank Averill, and Tom Hattox. The state of the art was punched cards, with separate codes to calculate potentials, energy bands, and construct the next iterative step in the SCF procedure. Reaching self-consistency required

submittal of multiple jobs. Nevertheless we and others got encouraging results as had DeCicco [35], Connolly [36], Mattheiss, Wood, Switendick [32], and others before us [37].

3.2. *The linearized augmented plane wave (LAPW) method*

The basic concepts and ideas of LAPW have been presented in various places [28,33,38] so only the main points shall be mentioned here. The energy dependence of the atomic-like radial functions can be treated in different ways. In the original APW this is done by choosing a fixed energy for each radial function, then doing the non-linear eigenvalue problem and laborious logarithmic derivative search just mentioned. In LAPW this energy dependence of each radial basis function $u_\ell(r, E)$ is linearized (that is, treated to linear order) according to Andersen's prescription [26]

$$A_{lm}(k_n)u_\ell(r, E_\ell) + B_{lm}(k_n)\dot{u}_\ell(r, E_\ell) \tag{6}$$

by taking a linear combination of a solution $u_\ell(r, E_\ell)$ at a fixed linearization energy E_ℓ (chosen at the centre of the corresponding band) and its energy derivative $\dot{u}_\ell = \partial u_\ell/\partial\varepsilon$ computed at the same energy. Each plane wave (labelled by k_n) is joined continuously (in value and slope) to the one-centre solutions inside the atomic sphere, thereby defining the relative weights of the u_ℓ and $\dot{u}_\ell$ contributions. The corresponding LAPW basis set is independent of the KS eigenvalues, hence allows determination of all the needed eigenvalues with a single diagonalization, in contrast with APW. Experience shows that the LAPW basis set also is sufficiently flexible to represent KS states near the linearization energy. The more strict constraint (value and slope) had the disadvantage that more PWs were needed to reach convergence. An early LAPW implementation (based on the MTA and without self consistency) was done by Koelling and Arbman [39]. Their program was the start for the WIEN code.

The LAPW method made it computationally attractive to go beyond the MTA, which into the 1970s still was frequently used. It worked reasonably well for highly coordinated (metallic) systems such as face centered cubic (fcc) metals. However, for covalently bonded solids, open or layered structures, or surfaces, the MTA is a poor approximation which can lead to serious discrepancies with experiment. Therefore it was important to treat the crystal potential (and charge density) without any shape approximation. The corresponding formalism was mainly done in the Freeman group [40]. The potential and charge density are expanded inside each atomic sphere into lattice harmonics (a symmetry-adapted linear combination of spherical harmonics)

$$\sum_{\mathrm{LM}} V_{\mathrm{LM}}(r)\, Y_{\mathrm{LM}}(r) \tag{7}$$

and as a Fourier series in the interstitial region:

$$\sum_{K} V_K e^{i\vec{K}.\vec{r}}. \tag{8}$$

This form is completely general, so such a scheme is termed a full-potential calculation. In order to have a small number of LM values in the lattice harmonics expansion, a local coordinate system for each atomic sphere is defined according to the point group symmetry of the corresponding atom. The transformation provides a rotation matrix which relates the local coordinates to the global coordinate system of the unit cell. The choice of sphere radii is not as critical in full-potential calculations as in the MTA. The difficulty in MTA is that one obtains different radii as optimum choice depending on whether one looks at the potential (maximum between two adjacent atoms) or the charge density (minimum between two adjacent atoms). Therefore in the MTA one must make a compromise but in full-potential calculations this problem is greatly reduced.

3.3. *Refinement of LAPW by local orbitals and going to an all-electron theory*

Core states are low in energy and the corresponding KS orbitals (or densities) are completely confined (practically speaking) within the atomic spheres. Thus one can treat them in an atomic approximation in the spherical part of the self-consistent potential and omit interactions with the neighbours. Valence states are high in energy with delocalized orbitals which are responsible for chemical bonding and form energy bands. There is, however, another type of orbitals which we call semi-core states. They have a lower energy than the valence states and reside mostly inside the spheres, but are not fully localized and have a 'core-leakage' of several per cent. Take the Ti atom as example. In it, the 1s, 2s and 2p are clear core states, followed by the semi-core states 3s and 3p, besides the valence states 3d, 4s, 4p. A severe restriction of the original LAPW method was that for each ℓ one could treat (due to the linearization) only one principle quantum number. In the present example one could not handle 3p and 4p Ti states at the same time. Singh [41] proposed the addition of local orbitals (LO) to the LAPW basis set in order to treat states with different principal quantum numbers (e.g. 3p and 4p states)

accurately while retaining orthogonality. In his scheme one solves the radial wave function at a low energy for the Ti-3p state but adds Ti-4p LAPW functions to force the corresponding LO to have zero value and slope at the sphere boundary thus enforcing the confinement. By adding such LOs (representing the main features of the Ti-3p states) to the LAPW basis set a consistent description of both the Ti-3p semi-core and the Ti-4p valence state is possible. A case for which this improvement is essential is the calculation of electric field gradients for TiO_2 (rutile) [42]. We discuss this in more detail in Section 6.4.

The concept of LOs fostered another idea, namely the APW plus local orbitals (APW + lo) method [43]. These local orbitals (lo) are denoted with lower case to distinguish them from the semi-core LOs just discussed. In APW + lo, one goes back to the APW basis but with the crucial distinction that the radial wave functions are at fixed energies. The variational flexibility needed in the basis to describe the energy dependence is obtained by means of additional local orbitals (lo). In this scheme the matching with the plane waves is again only done in value (as in the original APW). This makes the APW basis set much more efficient than the LAPW basis set in the sense of requiring only 50% as many plane waves. Therefore this new scheme is significantly faster (up to an order of magnitude) while keeping the convenience of LAPW [44]. The details of the three types of schemes (APW, LAPW, APW + lo) were described in [38]. A combination of the latter two schemes provides the basis for the new WIEN2k program [45].

As long as a solid contains only light elements, non-relativistic calculations are well justified, but as soon as a system of interest contains heavier elements, relativistic effects can no longer be neglected. In the medium range of atomic numbers (up to about 54) the so called scalar relativistic scheme is often used [46]. It describes the main contraction or expansion of various orbitals (due to the Darwin s-shift or the mass-velocity term), but omits spin-orbit interaction. The latter is really important for the heavy elements or when orbital magnetism plays a significant role. In the present version of WIEN2k the core states always are treated fully relativistically in a thawed core approximation. This means that they are recalculated for each SCF iteration in the given (spherical) potential by numerically solving the radial Dirac equation. For all other states, the scalar relativistic approximation is used by default, but spin–orbit interaction (computed in a second-variational treatment [47]) can be included if needed [48]. Since such a scheme makes use of the scalar relativistic radial basis functions, one can add a 'relativistic local orbital' (RLO) [49]. This corresponds to a $p_{1/2}$ orbital, which looks quite different from a non-relativistic or $p_{3/2}$ basis function. With these extensions nearly 100% of the relativistic effects can be recovered. For magnetic systems spin-polarized calculations must be performed as will be discussed in Section 6.6.

4. Computer development

In the 1960s the hardware situation was incomprehensibly different from today. The computer, on which K.S.'s PhD thesis was carried out in Vienna was a Datatron 205, part of which is exhibited at the Computer History Museum in Mountain View, California. This machine filled a room, had 1600 tubes (no transistors) and had a memory of 4080 words (with 44 bits). The input was made on paper tape (not even punch cards) and the programming was in machine language. The APW calculation (muffin-tin, non-SCF, with matrix sizes below 50×50) on ScC in the NaCl structure took many nights at this computer (see [34]). Now it would take a fraction of seconds on a laptop. When S.B.T. joined QTP, *the* University of Florida computer was an IBM 360/50. SCF iterations of the APW code were done a few at a time, overnight, with punched card inputs and source decks. By the time K.S. and S.B.T. wrote a paper together [50], we had a 360/65, but it was still punch cards and a few iterations a night. Let us skip 20 years and look at a PC that was available around 1985 but could hardly be used for APW calculations. Its price was about 20 times that of a present quad-core PC and had a memory of 512 kB and an external disk of 30 MB (instead of GB and TB nowadays). We went from main-frame computers to vector machines, mini-computers, then workstations, then PC clusters to present day high performance parallel computers. The present Vienna Scientific Cluster (156 in the top 500 list) consists of 3488 cores with 11.2 TB of available memory and has a peak performance of 36 TFlops. WIEN2k runs efficiently on this machine using 512 cores. The operating system in the old days was rather primitive and different for different vendors or hardware. In fact, the first version of WIEN was vectorized on an IBM 3090/400-2VF which ran IBM's VM/XA operating system. Now, for all practical purposes the Linux (Unix) operating system is ubiquitous. The programming language varied from machine language, Fortran66, Fortran IV, Fortran77 to Fortran90 (or C and C++). In addition, one now uses highly optimized mathematical libraries (BLAS, LAPACK) and parallelization tools like MPI for improving efficiency.

In earlier times, such routines were the responsibility of the code developers.

5. Algorithms, accuracy and efficiency

The setup and solution of the generalized eigenvalue problem is the main computational task for most electronic structure approaches. FLAPW and LAPW + lo are no exceptions. Thus the generalized eigenvalue probem must be optimally adapted to the available hardware. Cooperation with computer scientists and numerical mathematicians is extremely helpful. In order to reach high efficiency concepts like data locality, communications and band width must be considered carefully when choosing algorithms. For a representative example the setup of the spherical and non-spherical Hamilton (H) and Overlap (S) matrix elements might take only one-third of the time spent for diagonalization using efficient LAPACK/BLAS libraries. Diagonalization is the time determining step, as it scales like N^3 with the matrix size N. However, using the facts that (i) we often need only the lowest 10–20% of the eigenvalues, (ii) we do not really need a very accurate solution of the eigenvalue problem during the early SCF cycles, and (iii) we know that the matrices H and S change only modestly from one SCF cycle to the next, we can use an iterative diagonalization scheme. Such schemes use the eigenvalues and eigenvectors from the previous cycles to define a suitable subspace with a good preconditioner [51] and solve a smaller eigenvalue problem. If the preconditioner is efficient, an accurate solution can be obtained approximately at the same time that self-consistency also is reached. Typically, diagonalization time is then only 50% or less of the setup time and does not dominate the cpu time anymore. A very important point for an efficient code is to reach self-consistency for every possible system in as few cycles as possible. Originally one used straight (Pratt) mixing [52] between input and output density, but this would never converge for a complicated magnetic metal with several hundreds of d- or f-elements in the unit cell. Broyden's second method [53] or the recent multisecant version [54] of this scheme considers the information from previous iterations of the SCF as samples of a higher dimensional space to generate the new density for the next step. This was an important improvement for large systems and allows one to converge the h-BN/Rh(111) nanomesh [55], which has more than 1000 atoms in the unit cell, in about 30–40 iterations (see the discussion in Section 6.5). For some parts of the code sequential Fourier synthesis has been replaced by fast Fourier transforms (FFT), which do not dominate our calculations.

WIEN2k can treat all atoms in the periodic table with a similar effort, i.e. a heavy element like U requires similar effort to that for a light element like C. The high accuracy of WIEN2k comes from a balanced mixed basis set of plane waves and atomic functions, whose radial functions are recalculated numerically in the new potential at each SCF iteration. This allows them (in each iteration) to expand or contract according to the potential and ionicity (charge state). The main control of convergence with respect to basis size is via the parameter, $RK_{\max}$, the product of the smallest sphere radius R times the largest plane wave vector $K_{\max}$. Integration in reciprocal space requires a proper **k**-point mesh in the irreducible Brillouin zone (BZ). For small unit cells, metallic and magnetic systems, or some properties like optics (dielectric function ε) many (several thousands) **k**-points are needed, but these calculations can be done efficiently in parallel, even when only slow communication between the nodes is available. The larger the direct space unit cell grows the smaller the BZ becomes and thus fewer **k**-points (down to one) are needed, but then the matrix size can be so big that the matrices may not fit into memory of one processor. In this case MPI parallelization is necessary and the H and S matrices must be distributed over many nodes. For parallel computing, libraries like ScaLapack provide optimized eigensolvers.

For an efficient parallel code two features are important: the sequential part must be kept to an absolute minimum and the communication compared to the computing time should be small (sending large blocks). Consider a code which is parallelized only to 99%. Obviously, on 100 cpus only a speedup of 50 can be reached in such a situation. Our setup routine for the spherical part of H and S (at least 1/3 of the cpu time) is nearly 100% parallel and in practice has no communication. It scales near the theoretical limit up to 512 processors. On the other hand, linear algebra operations require some communications and they limit the parallelization depending on the speed of the network (presently Infiniband) and the size of the blocks stored on the individual nodes. For instance, a matrix of size 16,000 can be diagonalized efficiently only on up to 64–100 processors, while for a matrix size of 50,000 as many as 512 processors can be used. The scaling with system size N is still about N^3, which is typical for metallic systems. Codes with linear scaling are mostly restricted to insulators and short range interactions (leading to sparse matrices) and always will require a delicate balance between accuracy and efficiency. In contrast, from the beginning, the WIEN

strategy has been to provide a general code, not restricted to a class of materials by the constraints of certain scaling objectives.

6. Properties and applications

In this section diverse properties that can be obtained with WIEN2k will be illustrated for several selected examples and applications.

6.1. *Structure models*

We always describe the system structures using periodic boundary conditions. For bulk systems this simply means that the unit cell is infinitely repeated in all three dimensions. In comparison to real systems it should be stressed that all kinds of imperfections are ignored by this approach. Some of them can be simulated. For example, a defect can be studied by considering a supercell that consists of a $n \times n \times n$ cell of the original unit cell, where n is a small integer (about 2 to 4). When one atom in this larger unit cell is replaced by an impurity atom, the neighbouring atoms can relax to new equilibrium positions if symmetry allows it, otherwise the size of the supercell must be increased. Such a supercell is repeated periodically and represents an isolated impurity reasonably well provided that the supercell is big enough to suppress spurious impurity-impurity interactions. This example illustrates how theory can carry out computer experiments. For surfaces one can use the concept of a periodic slab which consists of a few (3–21) layers (commonly the thickness is chosen such that the central layer properties resemble bulk properties). These layers are separated from the periodically repeated ones by a sufficiently large empty region (representing vacuum) of about 10 Å (see the discussion of the nanomesh in Section 6.5). The super-cell approach is an idealization, but is a good approximation provided the cell is sufficiently large that the periodic images are effectively non-interacting. The structure model gets better the larger the super-cell is, but the computer time increases dramatically (order N^3).

While the first band structure codes could handle only rather simple cubic structures, for example the NaCl structure [34], nowadays all 230 space groups are available. The symmetry definitions may be taken from crystallography, for instance from the Bilbao Crystallographic Server (see www.cryst.ehu.es/cryst/) or the routines (provided by Vaclav Petricek from Prague) which are included in WIEN2k for that purpose. A symmetry analyzer (module SGROUP [56]) is also available, which finds the space group for a given set of atomic positions that were directly generated by the user in the input. Nowadays it is standard for bulk systems to have a crystallographic information file (CIF), which defines all the atomic positions. This information can be imported directly into WIEN2k. Such features become important when a unit cell contains many atoms and has low symmetry.

6.2. *Energy bands, density of states, band character*

The one-electron energy eigenvalues (solutions of the Kohn–Sham equation) as functions of **k**-vectors define the band structure. The **k**-mesh (the path along high symmetry lines in the irreducible Brillouin zone) can either be taken from some templates or generated graphically using XCrysDen [57]. The program that plots the energy bands is called 'spaghetti', in recognition of the fact that the raw eigenvalues can be difficult to interpret. There are some tools to help the analysis. An early illustration (1983) was a study of TiC, a refractory metal that is about as hard as diamond [58,59]. Figure 1(a) shows a section of the energy bands for TiC around the Fermi level using the PBE form of the GGA [17] XC functional. From the dispersion alone it is difficult to interpret these data: we are back to spaghetti.

In fact, these bands originate mainly from the C-2p and Ti-3d states. A symmetry analysis (contributed by Clas Persson, University of Uppsala) determines the irreducible representation and defines how the bands should be connected via compatibility relations and satisfaction of the non-crossing rule. An example is given in Figure 1(b). For example, the Δ_2, and Δ_5 band have predominantly Ti-d(t_{2g}) symmetry (see below).

For each eigenvalue $E_n(\mathbf{k})$, the modulus of the corresponding KS orbital ψ (E_{nk}) leads to an electron density that is normalized in the unit cell. This charge can be decomposed, by exploiting the LAPW basis set, into contributions from the region outside the spheres (interstitial) and from the atomic regions (labelled by the atom number t).

$$1 = q_{\text{out}} + \sum_{tl} q_{tl}. \tag{9}$$

The partial atomic charges within each atomic sphere, q_t, can be decomposed further into $q_{t\ell m}$ according to angular momentum ℓ and sometimes also m. This decomposition is very useful especially for analyzing the character of a band. The contributions from different m (for example the p_x, p_y, and p_z orbitals) can be distinguished provided they belong to a different class in the given point group. As an example let us take the d-orbitals of a transition metal in a cubic system, which are degenerate in the atom.

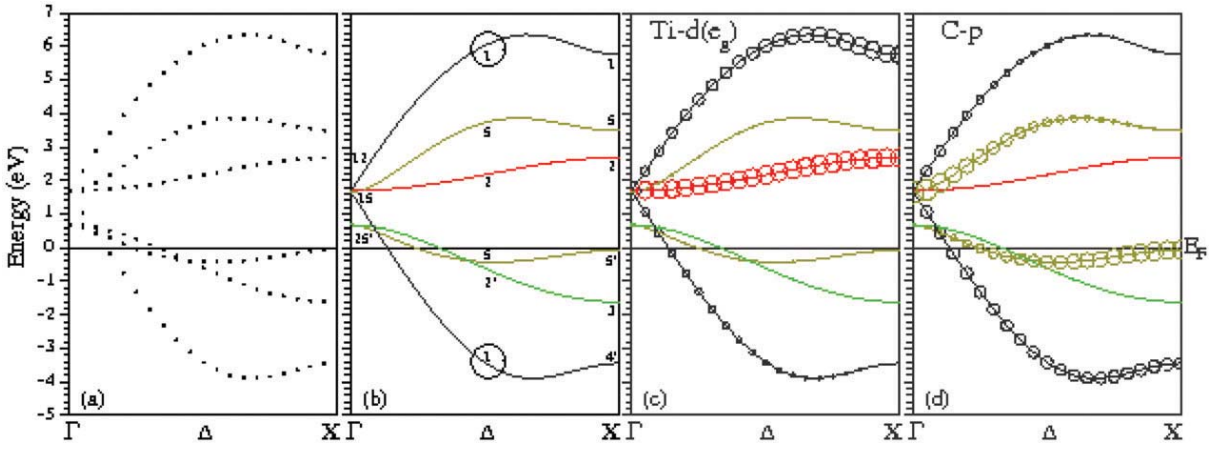

Figure 1. (Colour online) Energy bands of TiC along the high symmetry direction Γ-Δ-X. The energy (in eV) is taken with respect to the Fermi energy E_F: (a) E(**k**) as spaghetti, (b) bands labelled by irreducible representations, (c) character plot for Ti-d (e_g symmetry), (d) character plot of C-p.

When surrounded by ligands the five-fold degenerate d orbitals split into the t_{2g} and e_g manifold (crystal field splitting), for which the corresponding d-orbitals point between or towards the ligands, respectively. If one wants to know the character of states in the band structure, one can show character bands, sometimes called 'fat bands'. For each eigenvalue $E_n(\mathbf{k})$ one plots a circle with a radius proportional to the selected partial charge $q_{t\ell m}$. This technique is illustrated for TiC (Figure 1c and Figure 1d) by showing the Ti-d(e_g) and the C-p character of the bands, which varies along the high symmetry BZ direction Γ-Δ-X. For example, the highest band shown in Figure 1c and 1d starts out at Γ with a mixture between Ti-d and C-p but its character changes going towards X. The Ti contribution increases while that from C-p decreases. We will show another aspect in the next subsection by using the electron density.

From energy eigenvalues calculated on a sufficiently fine **k**-grid in the irreducible BZ one can obtain the density of states (DOS) often by means of the modified tetrahedron method [60]. By using information from the KS orbitals (partial charges, Equation (9)) one can also decompose the DOS into partial DOS, which are useful for the interpretation of chemical bonding and X-ray spectroscopy (see Section 6.7).

6.3. *Electron density*

In DFT the electron density plays the key role and thus we use it for another mode of interpretation. One can go from reciprocal space and a display of $E_n(\mathbf{k})$ to direct space and examine the electron density that corresponds to a given energy eigenvalue. (We could also show the KS orbital, but it is a complex function that is harder to visualize.) We continue with the 1983 illustration for TiC [58]. By examination of three eigenvalues along the Δ direction those authors could describe three types of covalent bonds, namely a C-p Ti-d σ, a Ti-d Ti-d σ and a C-p Ti-d π bond.

Here we repeat this analysis and show (Figure 2) how the corresponding electron density looks for one **k**-point, namely Δ (between Γ and X), and for two eigenvalues with Δ_1 symmetry (top and bottom bands in Figure 1(b), which are encircled). The Ti-d orbitals (of e_g symmetry) point towards C and form a C-p Ti-d σ bond. The reason that the density around carbon is spherically symmetric comes from the cubic symmetry: the p_x, p_y and p_z orbitals are equally occupied. At the lower Δ_1 energy (−3.4 eV), a bonding state is formed with a relatively high density between C and Ti, whereas at the higher Δ_1 energy (at +6.0 eV) the antibonding state appears with a node between Ti and C and thus zero density. In [58] it was shown that in the case of TiC all the bonding states are occupied but the antibonding one remained empty, which is the main reason for the high hardness of TiC. This is a system which is metallic and has covalent and ionic contributions making the bonding a mixture of these three bonding types (see also [57]).

In connection with charge transfer or ionicity one often wants to associate a charge with an atom in the system. Unfortunately such an association cannot be defined unambiguously and each procedure depends on the model. For instance, the well-known Mulliken charges depend on the basis set. In APW one easily can obtain the charges within the atomic spheres and the interstitial region, but these values clearly depend

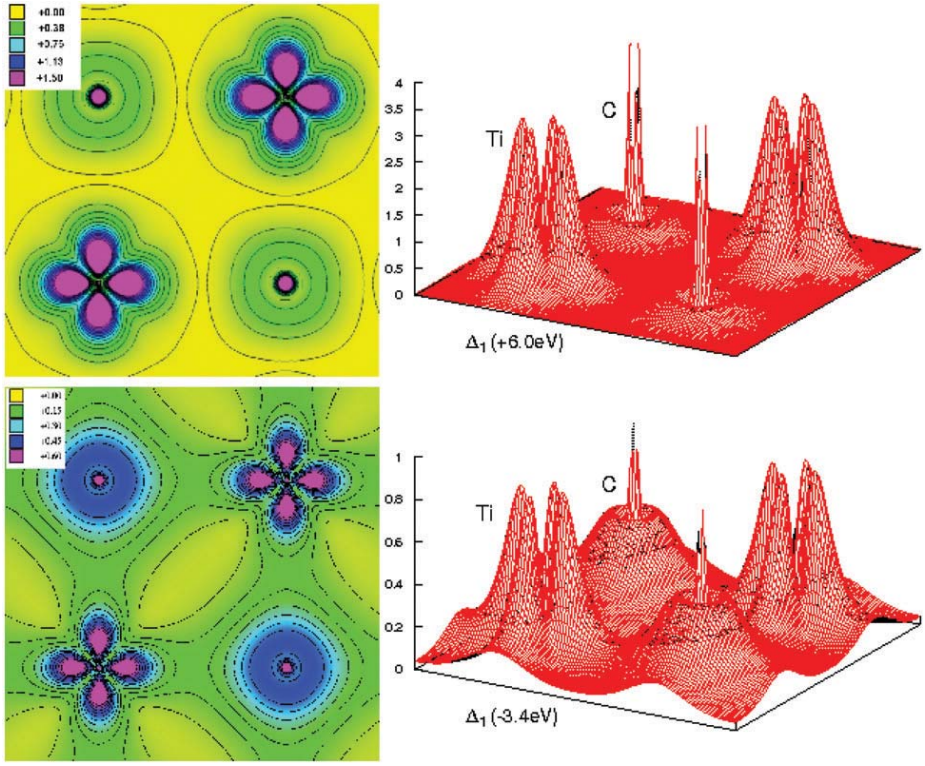

Figure 2. (Colour online) The electron density of TiC in the (100) plane is shown for the two states of Δ_1 symmetry corresponding to the bonding (at −3.4 eV) and antibonding (at +6.0 eV) C-p Ti-d σ bond (encircled in Figure 1(b)). The contour plots (left) were generated using XCrysDen [57].

on the choice of sphere radii. A more rigorously defined procedure, which is basis-set independent, is based on a topological analysis proposed by R. Bader [61], who called it atoms in molecules (AIM). This analysis divides space into uniquely defined atomic volumes ('basins') which contain exactly one nucleus by enforcing a zero-flux boundary:

$$\vec{\nabla}\rho \cdot \vec{n} = 0.$$

Recently this Bader charge analysis was used in connection with the Verwey transition in the double perovskite $YBaFe_2O_5$, in which one can distinguish between a charged order (CO) state (with Fe^{2+} and Fe^{3+}) and a valence-mixed (VM) state (also called mixed valence) in which Fe has the formal oxidation state of $Fe^{2.5+}$ [62] (Table 1).

In this system one needs to go beyond LDA or GGA and thus the authors [62] used GGA + U. It gives results that are consistent with experimental data when an effective U of around 7 eV is employed. From such a calculation for the CO phase there was a clear difference in the atomic charges associated with Fe for the two crystallographic sites, which correspond to Fe^{2+} and Fe^{3+}, whereas in the VM phase with only one type of Fe (with the formal oxidation +2.5) an AIM value in between these two values was obtained. These Bader charges typically are smaller than the formal (ionic) charges. For example for oxygen the formal charge would be −2, but the Bader charge is only around −1.4 electrons.

Table 1. Atomic charges using AIM for the charge ordered (CO) and valence mixed (VM) phase of $YBaFe_2O_5$ taken from [62]. GGA + U was employed with $U_{eff} = 7$ eV.

	CO	VM
Y	+2.17	+2.15
Ba	+1.51	+1.52
Fe (2+)	+1.36	
Fe (2.5+)		+1.62
Fe (3+)	+1.84	
O (average)	−1.38	−1.39

Chemical bonding changes the total electron density only by small amounts and thus the difference

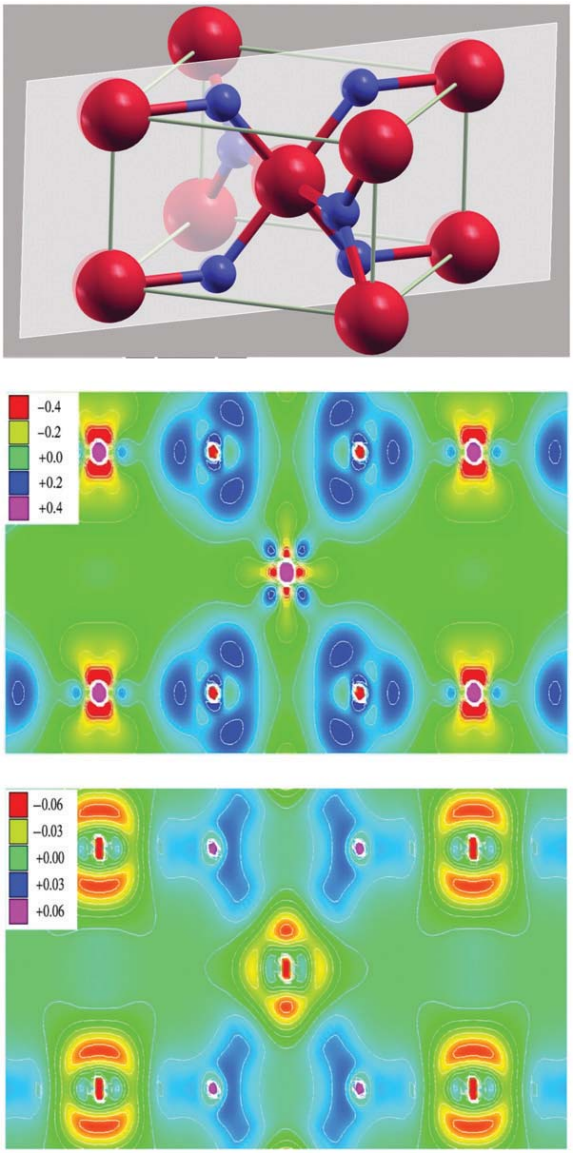

Figure 3. (Colour online) TiO_2 in the rutile structure: (a) the unit cell including the (110) plane through the 4 Ti atoms at the corners of the cell and the four oxygen atoms, which are at the Wyckoff positions corresponding to $(u, u, 0)$. The equivalent Ti in the centre has a local coordinate system that is rotated by 90° around the z-axis. In the (110) plane the difference electron density $\Delta\rho$ is taken between the SCF density and the corresponding superposed atomic densities: in (b) for the valence bands and in (c) for the semi-core states. The plots were generated using XCrysDen [57].

between the final SCF density and the superposition of free atomic densities (the start of an SCF cycle) shows the main reorganization due to bonding. This is the direct space analogue to the scheme in reciprocal space used in crystallography, namely comparison of structure factors with atomic form factors, the Fourier transforms of atomic charge densities. The difference density as a tool to find small details will be discussed for rutile TiO_2 in the next paragraph (see Figure 3 and its discussion).

6.4. *The electric field gradient*

Nuclei with a nuclear quantum number $I \geq 1$ have an electric quadrupole moment Q. The nuclear quadrupole interaction (NQI) stems from the interaction of such a moment Q and the electric field gradient (EFG), the second derivative of the Coulomb potential at the corresponding nuclear site. Measurements of the EFG can be done with nuclear magnetic resonance (NMR), nuclear quadrupole resonance (NQR), Mössbauer spectroscopy (MS) or perturbed angular correlations (PAC). The NQI allows determination of the product of Q and the EFG, denoted as Φ, a traceless tensor (with a principle component and an asymmetry parameter η), where e is the electronic charge and h Planck's constant

$$\nu \approx eQ\phi/h. \tag{10}$$

Up to about two decades ago, the EFG was mainly interpreted by a simple point charge model and corrections (Sternheimer factors). In several seminal papers [63–65] it was shown that the EFG originates mainly from the asymmetry of the (valence) electron density around the nucleus. The EFG is a ground state property that can be calculated directly within DFT. In a multipole expansion of the Coulomb potential only the $L = 2$ terms (Y_{LM}) contribute to the EFG, and, for instance, the component V_{zz} can be obtained from the charge density ρ by

$$Vzz = \int \frac{\rho Y_{20}}{r^3} \mathrm{d}r \tag{11}$$

where r is the distance from the nucleus. The factor r^3 strongly enhances the region around the nucleus. Often the EFG is very sensitive to small structural changes, in particular, distortions around the nucleus in question [66]. The ability to calculate EFGs has revolutionized this field and made it possible to learn more about bonding and structure relations. In many cases the agreement between theory and experiment is rather good.

For the most important Mössbauer isotope ^{57}Fe it became possible even to determine Q and change its accepted value by about a factor of two with respect to the prior literature value of 0.082 b. This was achieved by calculating EFGs for 16 Fe compounds (from insulators to magnetic compounds) and fitting the

Table 2. The high-temperature superconductor $YBa_2Cu_3O_7$ has four inequivalent oxygen sites. The partial 2p charges (in electrons) of their valence states are given in the first three columns and are labelled p_x, p_y, p_z (the smallest value is given in bold), where the Cartesian coordinates are assumed to be parallel to the crystallographic axes *a*, *b*, and *c*. The electric field gradient (EFG) components V_{aa}, V_{bb}, V_{cc} (labelled according to the axes *a*, *b*, and *c*) are given in units of $10^{21}\,V\,m^{-2}$ (the principal component is shown in bold). These data are taken from [68].

	p_x	p_y	p_z	V_{aa}	V_{bb}	V_{cc}
O(1)	1.18	**0.91**	1.25	−6.1	**18.3**	−12.2
O(2)	**1.01**	1.21	1.118	**11.8**	−7.0	−4.8
O(3)	1.21	**1.00**	1.118	−7.0	**11.9**	−4.9
O(4)	1.18	1.19	**0.99**	−4.7	−7.0	**11.7**

experimental NQI data with a new Q value of 0.16 b [67].

There are also cases as, for example, the high-temperature superconductor $YBa_2Cu_3O_7$, for which the EFG for Cu2, which lies in the layer where superconductivity occurs, differs by a factor of two from the experimental value. Nevertheless good agreement is obtained for Cu1, all the oxygen atoms and the Ba EFG [68]. This example illustrates that for highly correlated systems (as here for Cu2) the conventional approximate DFT functionals are not sufficient.

For the oxygen atoms in $YBa_2Cu_3O_7$, a physical interpretation was provided in [68], as is summarized in Table 2. In a case with equal orbital occupation numbers p_x, p_y, p_z the corresponding charge distribution would be spherically symmetric and the EFG would vanish. For the oxygen atoms the asymmetry in the charge distribution shows up in the p occupation numbers, where one orbital (shown in bold) is less occupied than the others. The orientation of this less occupied *p*-orbital coincides with the principal component of the EFG tensor (also shown in bold). For a physical interpretation we observe that the larger the asymmetry the higher the EFG for the four types of oxygen. The relative occupation of the *p*-orbitals can be traced back to the band structure. Take O1 as an example. It lies in the chain with Cu1 atoms along the y direction. In the x and z direction there are no nearest-neighbour atoms. Thus the orbitals are mostly non-bonding, hence fully occupied, which leads to values close to 1.2 electrons inside the oxygen sphere. The y orbital, however, interacts strongly with the neighbouring Cu1 atoms forming bonding and antibonding states. The latter are partly unoccupied leading to the smaller p_y occupation number of 0.91 electrons. This asymmetry in the occupation numbers causes an asymmetric charge distribution around the oxygen atom and thus an EFG. To a good approximation there is a proportionality (essentially the $\langle 1/r^3 \rangle$ expectation values of the corresponding orbital) between the EFG and a quantity, called asymmetry count $\Delta n_p = 1/2(p_x + p_y) - p_z$ relevant for the present case. If the asymmetry in the charge distribution originates from d orbitals, a similar expression exists (for further details see [68]).

In rutile (TiO_2) – the structure is shown in Figure 3(a) – agreement with experiment for the EFG could be obtained only when the semi-core states (from the Ti-3s and 3p shells) were included by means of local orbitals (LO) as discussed in [42] and mentioned in Section 3.3. Here we first discuss the difference electron densities (Figure 3). The EFG at the Ti site can be explained as partial cancellation between the 'on-site' semi-core and the 'off-site' Ti-4p contribution. In a simple picture one would ignore the semi-core states, since they correspond to filled shells with a spherically symmetric density which would have no contribution to the EFG. However, in reality the 'on-site' Ti-3p states are polarized by oxygen, where those *p*-orbitals pointing towards oxygen are depleted. Look for example at the central Ti in Figure 3(c) (bottom) where the p_z orbitals cause negative regions. In Figure 3(b) (centre) the $\Delta\rho$ from the valence bands is shown, which – first of all – shows the charge transfer from Ti to oxygen (positive and negative regions respectively). Next the asymmetry in the charge distribution around both types of atoms is obvious. The 'off-site' Ti 4p contributions correspond to the (orthogonalized) tails of the O 2s and 2p wave functions reaching into the Ti sphere, where they are expanded in partial waves. Therefore a larger p charge is found in orbitals pointing towards the oxygen atoms, and thus this 'off-site' contribution has a sign opposite to that of the 'on-site' part. Note that the scale in $\Delta\rho$ is much smaller for the semi-core than for the valence states but nevertheless both energy windows contribute to the EFG. Keep in mind the enhancement by the factor r^3 (Equation (11)). There is also a strong dependence of the EFG on structural changes namely the oxygen position $(u, u, 0)$ but that was already discussed in [42].

Next we discuss the main contributions to the Ti EFG (Table 3). First the contributions inside the Ti-sphere are given for the valence states, which include the O-2s, O-2p, Ti-3d, Ti-4s and Ti-4p states, then the semi-core (Ti-3s and 3p) states add up to their sum (third row). Then the small contribution originating from the interstitial region completes the total theoretical EFG, which is compared to two sets of experimental data. In addition to the EFG data,

Table 3. Contributions to the Ti electric field gradient (EFG) tensor (in units of $10^{21}\,\mathrm{V\,m^{-2}}$) of rutile TiO_2 are listed for (i) the valence (mainly Ti-4p), (ii) the semi-core (Ti-3s and 3p) states and (iii) the sum of the two but only inside the Ti sphere, (iv) interstitial region leading to (v) the total EFG from theory. In the next column the asymmetry parameter η is given. In the last two rows two experimental EFG data [69,70] are shown for comparison. The partial occupation (in number of electrons) of the Ti 4p and 3p orbitals for valence and core state are given in the last three columns.

	V_{xx}	V_{yy}	V_{zz}	η	p_x	p_y	p_z
Valence (4p)	+2.97	+3.83	−6.81		0.0812	0.0794	0.0988
Semi-core (3p)	−2.16	−2.41	+4.58		1.8871	1.8872	1.8763
Ti-sphere	+0.81	+1.42	−2.23				
Interstitial	−0.03	−0.06	+0.09				
Total EFG	+0.78	+1.36	−2.14	0.27			
Exp. [69]	+0.79	+1.49	−2.28	0.30			
Exp. [70]	+0.86	+1.34	−2.20	0.22			

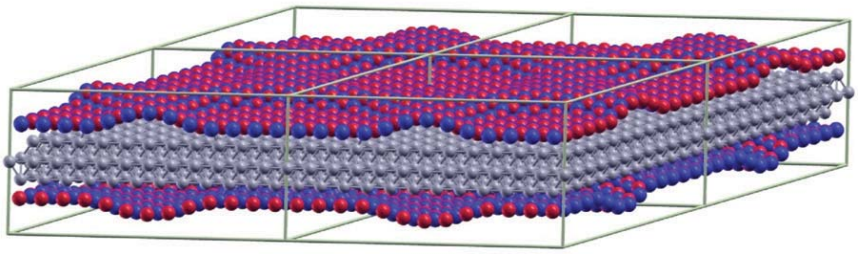

Figure 4. (Colour online) A 2×2 supercell representing h-BN and a Rh(111) surface. The boron (blue), nitrogen (red) and Rh (grey) atoms are shown. The single cell that is used in the calculation contains 1108 atoms. The plots were generated using XCrysDen [57].

the partial charges (inside the Ti sphere) corresponding to the Ti-4p and Ti-3p orbitals are listed.

A few comments are appropriate. Although the 4p charges (mainly representing the oxygen 'off-site' tails) are very small, the corresponding EFG contributions are large. For the semi-core states the charges are big as expected (for a filled shell) with a tiny anisotropy which causes a large EFGs due to the r^3 enhancement. Where does the V_{zz} come from in the valence region? Analysis shows that the value −6.81 (first row) originates almost entirely from the *p*-anisotropy while the *d*–*d* anisotropy, from a product of two *d*-like wave functions, (obvious in Figure 3) adds only less than 0.1 to the EFG. This comparatively small contribution comes about since the proportionality between charge anisotropy and EFG is the $\langle 1/r^3 \rangle$ expectation value. It is much smaller for the d orbitals than for p orbitals (for a discussion of the radial contributions to the EFG the reader is referred to the analysis on $YBa_2Cu_3O_7$ [68]). The importance of the semi-core states is obvious. It also has a significant effect on the oxygen EFG not shown here.

The EFG is also used in the study of other intricate systems, e.g. UO_2 [48], or $YBaFe_2O_5$ [62], where the details can be found in the corresponding literature.

6.5. *Total energy, forces and structure optimization*

The total energy (per cell in the periodic case) of a system can be obtained within DFT (according to Hohenberg–Kohn [15] and Kohn–Sham [6]). This quantity is needed for finding the relative stabilities of different structures (polymorphs, local structures at surfaces and the like). For structure optimization one searches for the equilibrium positions corresponding to the lowest energy, which is a big number. The derivative of the total energy with respect to the nuclear position defines the forces acting on the atom. For numerical reasons the knowledge of the forces helps significantly, since finding the equilibrium position of an atom, for which the forces vanish, often can be easier than looking for the total energy minimum.

$Y_2Nb_2O_7$ is one example for which the structure optimization had to follow a more complex route. The experimentalists [71] proposed a pyrochlore structure which can be described as corner-sharing empty Nb tetrahedra, where each Nb is octahedrally coordinated by O, with another network of Y tetrahedra. A DFT calculation [72] for this structure first led to metallic behaviour, in contradiction with experiment.

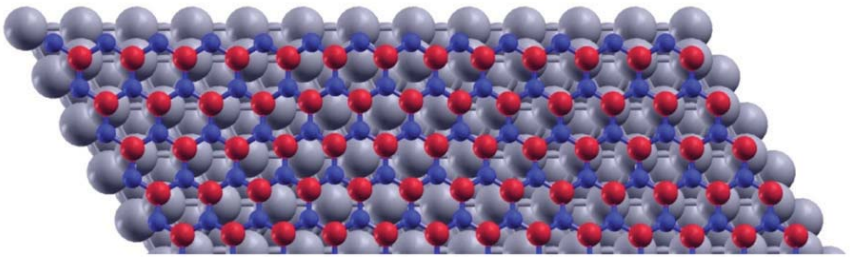

Figure 5. (Colour online) A section of the unit-cell (top view) showing the lattice mismatch between h-BN and the underlying Rh(111) surface (see also Figure 4) with a periodicity of 13×13 for the former but 12×12 for the latter. The plots were generated using XCrysDen [57].

For further analysis, the phonon dispersions of this compound in the ideal pyrochlore structure were calculated (using a real space force constant fitting based on forces calculated for atomic displacements in an 88 atom supercell). Several unstable modes (with imaginary phonon frequencies) corresponding to various charge and orbital orderings were found. If one follows these instabilities a lattice relaxation occurs in which the Nb atoms disproportionate to form a small and a large tetrahedron, corresponding to Nb^{5+} and Nb^{3+}, respectively. The relaxed structure is more stable than the original pyrochlore structure and the system becomes an insulator [72], in agreement with experiment.

A very challenging application was to solve the structural details of a regular nanomesh, formed when hexagonal boron nitride (h-BN) binds to a Rh(111) surface. There is a lattice mismatch between h-BN and Rh(111) of about 8%, with the result that 13×13 unit cells of h-BN match 12×12 unit cells of the underlying Rh(111). The atomic structure of this surface system has been unraveled by DFT calculations [55] to consist of a single, highly corrugated layer of h-BN. In order to simulate this complex structure, a slab was constructed containing three layers of Rh (corresponding to the three layers A, B, C of an fcc structure) and h-BN layers on both top and bottom (to keep inversion symmetry, which makes the matrices real instead of complex). This supercell (Figure 4) contains 1108 atoms and thus makes the calculation rather demanding but feasible nowadays.

The structure optimization started with a flat h-BN layer but allowed the atoms to relax, which led to a significant surface corrugation. The lattice mismatch can easily be seen in Figure 5 by looking at the top row of *N* atoms. At the left corner (or the right corner, the periodic image) nitrogen sits on top of Rh, a favourable positions with respect to the underlying Rh (leading to a small distance between Rh and h-BN). However, going from left to right one can see that *N* comes to other, less-favourable positions. Looking at the fourth row of *N* atoms (around the fifth and sixth *N* from left) one sees a region where *N* lies above a hollow position of the underlying Rh surface, a rather unfavourable situation causing a larger separation from the Rh surface. The B atoms have attractive forces towards Rh (with bonding orbitals) whereas for *N* the repulsive forces dominate (due to the occupation of antibonding orbitals). This mechanism causes a corrugation that can be seen in Figure 4 with low and high regions of h-BN. Once the structure is unraveled, other experimental data can be explored, for example data from scanning tunneling microscopy (STM), X-ray absorption spectroscopy, or N-1s core level shifts as discussed in [55,73]. The computational challenge should be reiterated: this is a metallic system with a surface and more than 1000 atoms per cell.

6.6. *Magnetism*

For magnetic systems, spin-polarized calculations must be performed. The default is collinear magnetic order. Rather than just the electron density, one needs the spin densities (for spin-up and spin down electrons) or the total density plus the magnetization density (difference of spin densities). This information is used either for the LSDA (local spin density approximation) or the GGA functionals. Spin-polarized calculations allow the study of ferromagnetic materials like Fe, Co, Ni or antiferromagnets like Cr. If one is interested in the orientation of the magnetic moments with respect to the crystal structure, the spin–orbit interaction must be included. It definitely is needed for heavier elements or when orbital moments become important. An example is the calculation of the magneto-crystalline anisotropy energy (MAE) as illustrated for the double perovskite $YBaFe_2O_5$ [62].

The total energy of this system is 115 578.240 Ryd but the MAE difference between different orientations is a fraction of a mRyd, which means that the quantity of interest is in the tenth decimal.

Half-metallic systems are receiving increasing attention in connection with spintronics applications, in which one spin type should be injected into a device. An early example was CrO_2 crystallizing in the rutile structure, which was predicted to be a half metal [74]. In such systems, the spin-up electrons are in a metallic state, whereas the spin-down electrons have bands with a gap. A character band representation (as discussed in Section 6.2) of these bands is provided in [38].

One recent application [75] to a rather complex system was PrO_2, which has a CaF_2 structure. It shows a Jahn–Teller distortion, contains Pr-4f electrons which form a localized band (lower Hubbard band) for one electron but hybridize with the other valence electrons with about 0.6 f-electrons and thus is in between Pr^{3+} and Pr^{4+}, is magnetic and an insulator requiring a relativistic treatment. A GGA + U calculation found results that are consistent with all available experimental data (gap, moment, EFG, distortion). For further details the reader is referred to the original paper [75]. This system has only a few atoms per unit cell but has an enormous complexity.

A non-collinear spin density extension to WIEN2k is available too, which for example was applied to UO_2 [48]. In this case the orientation of the magnetic moments varies throughout the unit cell.

6.7. *Optics, spectroscopy and other properties*

As we mentioned already, except for the highest occupied one, KS energy eigenvalues have no formal sanction as excitation energies. Nonetheless they are used frequently as estimates of spectroscopic properties. For example the energy gaps of insulators are typically underestimated by about 50% in LDA/GGA calculations. This was already known from early APW calculations with Xα [25] and it was argued [23] that even the exact Kohn–Sham gap misses the integer discontinuity Δ_{XC}. Better estimates of the quasiparticle spectrum can be obtained by GW calculations (employing many body perturbation theory) [76] or by the so called hybrid-DFT schemes, in which a certain fraction of single-determinant exchange (which overestimates gaps) is combined with a GGA functional. Such hybrid systems are presently implemented in WIEN2k. However non-local single-determinant exchange is rather difficult to compute in a periodic system and consequently hybrid computations are much more demanding than those with ordinary XC functional.

Recently, a local potential called the modified Becke–Johnson (MBJ) potential was proposed [77], which is probably the first local potential that yields energy band gaps close to experiment. It has an accuracy similar to (or sometimes even better than) very expensive GW calculations. The MBJLDA potential is based on an approximate Slater-potential (as local approximation to Hartree–Fock) and a screening term and uses the density, its gradient, the Laplacian and the kinetic energy density τ as input. The relative strength of the various terms is determined from an average of $\nabla\rho/\rho$ and thus no element specific input is needed. It works for small gap semiconductors (Ge, Si, InSe) as well as for large gap insulators like LiF or even Ne. Even more surprising, it also works for the class of 'highly correlated TM-oxides' like MnO or NiO and improves the gap much more than non-self-consistent GW calculations. It was argued that a local potential can never obtain proper gaps but we found that in practice it works. A possible explanation is that in all known cases the orbitals of the valence and conduction bands are located in different spatial regions (e.g. localized around an atom or delocalized in the interstitial region; different symmetries like d-orbitals of t_{2g} or e_g symmetry) and thus even a local potential can affect these distinct orbitals differently.

Optical excitations in solids commonly are described in the independent particle approximation (IPA) using the quasi-particle states of DFT calculations. Starting with the joint density of states one can include the transition probability between states nk and n′k (at a given k) by calculating the squared momentum matrix elements $M = |\langle n'k|A.p|nk\rangle|^2$ to obtain the imaginary part of the dielectric function ε_2 [78]. By means of a Kramers–Kronig transformation the real part ε_1 can be obtained and from this knowledge of ε other optical properties (conductivity, reflectivity or the loss function) can be calculated.

However, sometimes (in particular for insulators) the frequency dependent dielectric function ε in the IPA may have little in common with the experimental situation because excitations are a two-particle process and the missing electron-hole correlation can affect the calculated optical response of a material significantly when these excitonic effects are strong. In order to overcome this problem, one needs to include the electron–hole correlation explicitly by solving the Bethe–Salpeter equation (BSE) [79], where one can use the WIEN2k orbitals as input. A detailed discussion concerning various aspect of the BSE formalism, as well as alternative approaches employing time

dependent density-functional theory (TDDFT) can be found, e.g. in [80].

Core-level spectroscopies like X-ray emission or X-ray absorption also can be obtained in WIEN2k because of the all-electron nature of this package. In X-ray emission one measures a dipole transition between a valence and a core state. According to the $\Delta\ell$ selection rules such spectra provide information on the local (specific to the atom in which the core state resides with angular momentum ℓ) and partial '$\ell \pm 1$' density of states of the occupied (valence) states [81]. Alternatively, the fine structure of X-ray absorption spectroscopy (XAS, XANES, NEXAFS) gives similar information about the unoccupied (conduction band) states. However, there is an important difference, since the final state in XAS has a core hole, which can (due to excitonic effects) severely affect the calculated spectrum. Since these core holes are rather localized, one can simulate these effects by a super-cell approach, where a core electron is removed from one of the atoms in the supercell, which is solved self-consistently. The resulting partial DOS at this atom resembles the experimental spectra much better than does the ground state partial DOS [82]. Electron energy loss spectroscopy (EELS) is closely related to XAS. In EELS, the momentum of the electron plays an analogous role to the polarization vector of the X-rays. A separate module TELNES [83] exists in WIEN2k which allows a detailed simulation of EELS spectra considering all kinds of experimental settings and including possible quadrupolar transitions.

For some properties like the hyperfine interaction parameters, high accuracy is needed close to the nucleus. In such a case the numerical basis functions in LAPW are clearly superior to schemes involving Gaussians or pseudo-wave functions for example. Besides the EFG discussed in Section 6.4, isomer shifts or magnetic hyperfine fields (HFF) for Mössbauer spectroscopy also can be obtained. Isomer shifts are proportional to the difference of the electron density at the nucleus between source and absorber and therefore need a nuclear calibration constant α, which depends on the nuclear size changes during the Mössbauer transition. The HFF originates from three terms. The first one, often dominant, is proportional to the spin-density at the nucleus, whose main contribution usually comes from the core electrons that are polarized proportional to the local 3d (4f) moment. When spin-orbit interaction is taken into account [84], the other contributions due to the dipolar field and the orbital contribution (proportional to the orbital moment) can also be included.

A transformation from a Bloch-picture to a Wannier description can also be desirable for interpretation, for extraction of hopping parameters or for subsequent dynamical mean field (DMFT) calculations for correlated electrons. Recently an interface [85] between Wien2k and Wannier90 [86] has been developed. It supports convenient generation of Wannier functions from Wien2k Bloch states.

The WIEN2k code provides many tools to compute a large variety of properties and results, from energy bands, DOS, electron and spin densities, magnetic moments, optical spectra, total energies, forces, EFG, HFI, spin–orbit coupling, etc. Often a combination is needed in order to gain insight into a specific material. Sometimes different functionals or extensions beyond DFT are needed in order to get agreement with experimental data.

Pressure is an easy parameter for DFT calculations (see for example [87]) in contrast to experiments. The opposite is true for estimating temperature effects which are easier to obtain in experiment than for theory. Finite temperature effects can be included using lattice vibrations, which may be approximated from phonon data.

7. Distribution of the code

Porting and distributing the WIEN2k code (see www.wien2k.at) has a long history from the first Vienna version on paper tape, to punch cards at QTP, then large magnetic tapes and now the graphical user interface w2web (wien to web). In 1988 S.B.T. had the chance to get an IBM 'vector code conversion project' grant for the three authors. P.B. and K.S. came to Gainesville and we vectorized the code, developed a set of test cases, and wrote the original documentation. From the start we had agreed to distribution of the source. In fact, that was a part of the IBM contract. The first version was made available in our publication with P. Sorantin [30], where the code was given the name WIEN (the German name for Vienna) because that is where the code was started. With rapid changes new releases came out, namely WIEN93, WIEN95, WIEN97 but in the year 2000 (year 2k) the code was renamed WIEN2k the name that has persisted. The program started out from a single user but now is distributed worldwide (with more than 1600 licenses) among academic, governmental, and industrial user groups. Following the spirit of QTP, the source code continues to be made available, thereby encouraging various researchers to develop new features. Such features usually are made available to the WIEN2k community. Special thanks should go to all who have contributed. This large number of users has helped both, to make the program portable to many hardware

platforms as well as to find and fix bugs. A mailing list helps novice users to find solutions provided by experienced users. Another framework that turned out to be very practical are the so called WIEN workshops which were held since 1995, many of them in Vienna but also in Trieste, Italy (1998), in Esfahan, Iran (2002), Penn State (2002, 2004, 2007, 2009), Kyoto, Japan (2005), Los Angeles (2005), Singapore (2007) and Nantes, France (2010). In 2006 Shinya Wakoh published a book on WIEN2k in Japanese. In the solid state community WIEN2k has been established as benchmark code for other software packages. For example, S.B.T. uses results from it from time to time to check really hard GTO calculations.

8. Summary and conclusion

DFT calculations with approximate functionals can provide extremely useful information concerning the electronic structure of ordered crystal structures and surfaces. Hypothetical or artificial structures can be considered and their properties, irrespective whether they exist experimentally or not, can be calculated. Information concerning the electronic, optic or magnetic properties becomes available. Such calculations can predict whether a system is an insulator, a metal or is magnetic. Chemical bonding can be analysed, thus enabling prediction of how the system may change with deformations, under pressure, or substitutions. The examples given above are just a small selection to illustrate some possibilities DFT, as embodied in the WIEN2k code, can provide.

The combination of algorithmic developments and increased computer power has led to a significant improvement in the ability to simulate relatively large systems on proper computer hardware. At present systems containing about 1000 atoms per unit cell can be handled but such calculations do need a parallel computer with fast communication. Small systems (below 100 atoms) often can be treated efficiently on PCs or a cluster of PCs instead of the powerful workstations or supercomputers that were needed about a decade ago.

It should be mentioned that other schemes of comparable quality to solve the KS equation are available too, e.g. modern pseudo-potentials or other full-potential methods. However, there are also simplified versions of electronic structure calculations in which additional approximations are made to speed up the code, but often they may not provide high enough accuracy to study details of the electronic structure.

In the spirit of the Sanibel Symposia and the Quantum Theory Project (QTP) in general, progress in code development comes from the combination of chemistry, physics, material sciences, numerical mathematics, or computer science to mention the important ones. One needs many aspects such as formalism, new DFT functionals, but also implementation into a code, efficiency, portability, symmetry (group theory) leading to specific results that can be directly compared with experiments. The many fruitful discussions and the available expertise have laid the ground for the ambitious project that eventually led to WIEN2k.

Over the last forty years or more, dramatic improvements were achieved. Method developments had several important consequences. In the early stages several severe approximations had to be made and thus it was not clear, if disagreement was found (either between two codes or between theory and experiment), what caused the discrepancy. Nowadays when a calculation is carried out with DFT, a suitable approximate functional, an extensive basis set, a good k-mesh, with full potential, with all electrons, and with inclusion of relativistic effects, then one can say that the problem is solved properly. Investigating a problem with two independent computer codes, which use the same structure model and the same DFT functional, will find essentially the same results (provided both calculations are well converged as just mentioned). If disagreement with experiment occurs then either the structure model is inappropriate or the quantum mechanical treatment (choice of DFT functional) is not adequate. In the time of MTA without relativistic effects this certainly was not the case. The present situation has given theory much more predictive power than twenty years ago.

Future developments seem likely to go in the following directions: improvement of the quantum mechanical treatment (new functionals, hybrid schemes or even beyond DFT), inclusion of other properties (e.g. chemical shifts), adaptation to new hardware (cell processors), and enlarging the system size (beyond 1000 atoms per unit cell) to simulate realistic solids with impurities or defects.

Acknowledgements

The authors express their thanks to the many people who have contributed to the development of the WIEN2k code (in particular L.D.Marks, and R.Laskowski for the most recent improvements) and its antecedents. SBT stand for the initials of the three authors but also for the third author, who thought up the Gainesville part of this project. He knew what his friends, K.S. and P.B., were doing in Vienna. The long-term friendship among SBT made it possible that WIEN2k is a success story. S.B.T. (the individual) acknowledges support from US Dept. of Energy grant DE-SC-0001239.

References

[1] http://nobelprize.org.
[2] R.J. Bartlett and M. Musial, Rev. Mod. Phys. **79**, 291 (2007); O. Sode, M. Keçeli, S. Hirata and K. Yagi, Int. J. Quantum Chem. **109**, 1928 (2009).
[3] J.W.D. Connolly, Mol. Phys. (this volume).
[4] J.C. Slater, Phys. Rev. **81**, 385 (1951).
[5] R. Gaspar, Acta Phys. Acad. Sci. Hungary **3**, 263 (1954).
[6] W. Kohn and L.S. Sham, Phys. Rev. **140**, A1133 (1965).
[7] J.C. Slater and J. Wood, Int. J. Quantum Chem. **4S**, 3 (1972).
[8] K. Schwarz, Phys. Rev. B **5**, 2466-8 (1972).
[9] K. Schwarz, Theoretica Chemica Acta **34**, 225 (1972).
[10] K. Schwarz and F. Herman, J. Phys. **C3**, 277 (1972).
[11] T. Koopmans, Phys. **1**, 104 (1933).
[12] J.F. Janak, Phys. Rev. B **18**, 7165 (1978).
[13] K. Schwarz, Chem. Phys. **7**, 100 (1975).
[14] C. Görannson, W. Olovsson and I.A. Abrikosov, Phys. Rev. B **72**, 134203 (2005).
[15] P. Hohenberg and W. Kohn, Phys. Rev. **136B**, 864 (1964).
[16] C.M. Ceperley and D.J. Alder, Phys. Rev. Lett. **45**, 566 (1980).
[17] J.P. Perdew, K. Burke and M. Ernzerhof, Phys. Rev. Lett. **77**, 3865 (1996).
[18] J.P. Perdew, S. Kurth, A. Zupan and P. Blaha, Phys. Rev. Lett. **82**, 2544 (1999).
[19] P. Haas, F. Tran, P. Blaha, K. Schwarz and R. Laskowski, Phys. Rev. B **80**, 195109 (2009).
[20] P. Haas, F. Tran, P. Blaha, S. Pedroza, J.R. da Silva, M. Odashima and K. Capelle, Phys. Rev. B **81**, 123136 (2010).
[21] P. Novak, F. Boucher, P. Gressier, P. Blaha and K. Schwarz, Phys. Rev. B **63**, 235114 (2001).
[22] J. Heyd, J.E. Peralta, G.E. Scuceria and R.L. Martin, J. Chem. Phys. **123**, 174101 (2005).
[23] F. Tran, P. Blaha, K. Schwarz and P. Novak, Phys. Rev. B **74**, 155108 (2006).
[24] S.B. Trickey, F.R. Green Jr and F.W. Averill, Phys. B **8**, 4822 (1973).
[25] S.B. Trickey, J.A. Alford and J.C. Boettger, in *Computational Materials Science*, vol. 15 of *Theoretical and Computational Chemistry*, edited by J. Leszczynski (Elsevier, Amsterdam, 2004), pp. 171–228.
[26] O.K. Andersen, Phys. Rev. B **12**, 3060 (1975).
[27] A.R. Williams, J. Kübler and C.D. Gelatt Jr, Phys. Rev. B **82**, 6094 (1979).
[28] D.J. Singh and L. Nordström, *Plane Waves, Pseudopotentials and the LAPW method*, 2nd ed (Springer, New York, 2006), ISBN 10:0-387-28780-9.
[29] W. Kohn, in *Many Body Theory*, edited by R. Kubo (Syokabo, Tokyo, and Benjamin, NY, 1966), Vol. I, pp. 73–85.
[30] P. Blaha, K. Schwarz, P. Sorantin and S.B. Trickey, Comput. Phys. Commun. **59**, 399 (1990).
[31] J.C. Slater, Phys. Rev. **51**, 846 (1937).
[32] L.F. Mattheiss, J.H. Wood and A.C. Switendick, in *Methods in Computational Physics*, edited by B. Alder, S. Fernbach, and M. Rotenberg (Academic, New York, 1968), Vol. 8, pp. 64–147.
[33] K. Schwarz and P. Blaha, Comput. Mater. Sci. **28**, 259 (2003).
[34] K. Schwarz, P. Weinberger and A. Neckel, Theoretica Chemica Acta **15**, 149 (1969).
[35] P.D. DeCicco, Phys. Rev. **153**, 931 (1967).
[36] J.W.D. Connolly, Phys. Rev. **159**, 415 (1967).
[37] J.C. Slater, J.B. Mann, T.M. Wilson and J.H. Wood, Phys. Rev. **184**, 672 (1969).
[38] K. Schwarz, P. Blaha and G.K.H. Madsen, Comput. Phys. Commun. **147**, 71 (2002).
[39] D.D. Koelling and G.O. Arbman, J. Phys. **F5**, 2041 (1975).
[40] E. Wimmer, H. Krakauer, M. Weinert and A.J. Freeman, Phys. Rev. B **24**, 4571 (1982).
[41] D.J. Singh, Phys. Rev. B **43**, 6388 (1991).
[42] P. Blaha, D.J. Singh, P.I. Sorantin and K. Schwarz, Phys. Rev. B **46**, 1321 (1992).
[43] E. Sjöstedt, L. Nordström and D.J. Singh, Solid State Commun. **114**, 15 (2000).
[44] G.H.K. Madsen, P. Blaha, K. Schwarz, E. Sjöstedt and L. Nordström, Phys. Rev. B **64**, 195134 (2001).
[45] P. Blaha, K. Schwarz, G.K.H. Madsen, D. Kvasnicka and J. Luitz, *An Augmented Plane Wave Plus Local Orbitals Program for Calculating Crystal Properties* (Vienna University of Technology, Austria, 2001), ISBN 3-9501031-1-2.
[46] D.D. Koelling and B.N. Harmon, Solid State Phys. **10**, 3107 (1977).
[47] A.H. MacDonnald, W.E. Pickett and D.D. Koelling, J. Phys. C: Solid State Phys. **13**, 2675 (1980).
[48] R. Laskowski, G.K.H. Madsen, P. Blaha and K. Schwarz, Phys. Rev. B **69**, 140408 (2004).
[49] J. Kunes, P. Novak, R. Schmid, P. Blaha and K. Schwarz, Phys. Rev. B **64**, 153102 (2001).
[50] T.J. Kuebbing, K. Schwarz, S.B. Trickey and J.B. Conklin Jr, Phys. Rev. Lett. **26**, 1251 (1971).
[51] P. Blaha, H. Hofstätter, O. Koch, R. Laskowski and K. Schwarz, J. Computat. Phys. **229**, 453 (2010).
[52] G.W. Pratt, Phys. Rev. **88**, 1217 (1952).
[53] D.J. Singh, H. Krakauer and C.S. Wang, Phys. Rev. B **34**, 8391 (1986).
[54] D.L. Marks and D.R. Luke, Phys. Rev. B **78**, 075114 (2008).
[55] R. Laskowksi, P. Blaha, Th. Gallauner and K. Schwarz, Phys. Rev. Lett. **98**, 106802 (2007).
[56] B. Yanchitzky and T. Timoshevskii, Comput. Phys. Commun. **139**, 235 (2001).
[57] A. Kokalj, J. Mol. Graphics Modelling **17**, 176 (1999).
[58] P. Blaha and K. Schwarz, Int. J. Quantum Chem. **23**, 1535 (1983).
[59] P. Blaha, J. Redinger and K. Schwarz, Phys. Rev. B **31**, 2316 (1985).

[60] P.E. Blöchl, O. Jepsen and O.K. Andersen, Phys. Rev. B **49**, 16223 (1994).
[61] R. Bader, *Atoms in Molecules: A Quantum Theory* (Oxford University Press, New York, 1994).
[62] C. Spiel, P. Blaha and K. Schwarz, Phys. Rev. B **79**, 115123 (2009).
[63] P. Blaha, K. Schwarz and P. Herzig, Phys. Rev. Lett. **54**, 1192 (1985).
[64] K. Schwarz and P. Blaha, Z. Naturforsch. **A47**, 197 (1992).
[65] P. Blaha, K. Schwarz, W. Faber and J. Luitz, Hyperfine Int. **126**, 389 (2000).
[66] M. Body, C. Legein, J. Buzare, G. Silly, P. Blaha, C. Martineau and F. Calvagrac, J. Phys. Chem. A **111**, 11873 (2007).
[67] P. Dufek, P. Blaha and K. Schwarz, Phys. Rev. Lett. **75**, 3545 (1995).
[68] K. Schwarz, C. Ambrosch-Draxl and P. Blaha, Phys. Rev. B **42**, 2051 (1990).
[69] C. Gabathuler, E.H. Hundt and E. Brun, in *Magnetic Resonance and Related Phenomena* (North Holland, Amsterdam, 1973), p. 499.
[70] O. Kanert and H. Kolem, J. Phys. C **21**, 3909 (1988).
[71] Y. Maeno, H. Hishimoto, K. Joshyda, S. Nishizaki, P. Fujita, J.G. Bednorz and F. Lichtenberg, Nature **372**, 532 (1994).
[72] P. Blaha, D.J. Singh and K. Schwarz, Phys. Rev. Lett. **93**, 216403 (2004).
[73] R. Laskowksi and P. Blaha, Phys. Rev. B **81**, 075418 (2010).
[74] K. Schwarz, J. Phys. F: Met. Phys. **16**, L211 (1986).
[75] F. Tran, J. Schweifer, P. Blaha, K. Schwarz and P. Novák, Phys. Rev. B **77**, 085123 (2007).
[76] M. Shishkin and G. Kresse, Phys. Rev. B **75**, 235102 (2007).
[77] F. Tran and P. Blaha, Phys. Rev. Lett. **102**, 226401 (2009).
[78] C. Ambrosch-Draxl and J. Sofo, Comput. Phys. Commun. **175**, 1 (2006).
[79] R. Laskowski, N.E. Christensen, P. Blaha and B. Palanivel, Phys. Rev. B **79**, 165209 (2009).
[80] G. Onida, L. Reining and A. Rubio, Rev. Mod. Phys. **74**, 601 (2002).
[81] K. Schwarz, J. Phys. C.: Solid State Phys. **10**, 195 (1977).
[82] V.N. Strocov, T. Schmitt, J. Rubensson, P. Blaha and P.O. Nilsson, Phys. Stat. Sol. (b) **241**, R27 (2004).
[83] C. Hebert, P.H. Louf, P. Blaha, M. Nelhiebel, J. Luitz, P. Schattschneider, K. Schwarz and B. Jouffrey, Ultramicroscopy **83**, 9 (2000).
[84] P. Blaha, J. Phys.: Conf. Ser. (in print).
[85] J. Kunes, R. Arita, P. Wissgott, A. Toschi, H. Ikeda, K. Held, Comput. Phys. Commun. (forthcoming) arXiv:1004.3934v1.
[86] A.A. Mostofi, J.R. Yates, Y.-S. Lee, I. Souza, D. Vanderbilt and N. Marzari, Comput. Phys. Commun. **178**, 685 (2008).
[87] J.A. Nobel, S.B. Trickey, P. Blaha and K. Schwarz, Phys. Rev. B **45**, 5012 (1992).